Jpn. J. Appl. Phys. Vol. 38 (1999) pp. 4404–4415
Part 1, No. 7B, July 1999

Hybrid Modeling of a Capacitively Coupled Radio Frequency Glow Discharge in Argon: Combined Monte Carlo and Fluid Model

Annemie BOGAERTS*, Renaat GIJBELS and Wim GOEDHEER[1]

University of Antwerp, Department of Chemistry, Universiteitsplein 1, B-2610 Wilrijk-Antwerp, Belgium
[1]*FOM-Institute for Plasmaphysics "Rijnhuizen", P.O. Box 1207, 3430 BE Nieuwegein, The Netherlands*

(Received November 16, 1998; accepted for publication March 29, 1999)

A hybrid model has been developed for a capacitively coupled rf glow discharge in argon, employed as a spectroscopic source in the field of analytical chemistry. The cell is a rather small cylinder with a very small rf-powered electrode (only 5 mm in diameter). The typical working conditions applied for analytical spectroscopy are a gas pressure of 6 Torr and incoming power of 10 W. The hybrid model consists of a Monte Carlo model for the electrons and a fluid model for the electrons and argon ions. The latter model also contains Poisson's equation, to obtain a self-consistent electric-field distribution. The input values for the model are the gas pressure, the discharge power, the cell geometry and the collision cross sections. The typical calculated results include the rf and dc bias voltage, the electrical current at the rf electrode, the potential distribution, the density of argon ions and electrons, the electron energy-distribution function and information about the collision processes of the electrons. These results are presented throughout the discharge cell and as a function of time in the rf cycle. Moreover, we have investigated how many rf cycles have to be followed with the Monte Carlo model before a periodic steady state is reached.

KEYWORDS: modeling, Monte Carlo, fluid model, glow discharge, radio frequency, argon, plasma, computer simulation

1. Introduction

Glow discharges have increasing interest in a large number of application fields, *e.g.*, in the microelectronics industry (plasma etching of surfaces, deposition of thin films), flat plasma display panel technology, the laser and light industry, and also in analytical spectrochemistry.[1,2] In the latter application, the cathode (or the rf-powered electrode) of the glow discharge is fabricated from the material to be analyzed. The bombardment of fast ions and atoms from the plasma on the cathode causes the release of cathode atoms (i.e., by sputtering). These sputtered atoms arrive in the plasma and are subject to collisions. Excitation collisions (and the subsequent radiative decay) give rise to photons characteristic of the material to be analyzed, which can be detected by optical emission spectrometry. Ionization collisions create ions of the material to be analyzed, which can be measured by mass spectrometry.

Since the sample to be analyzed acts as the cathode in the glow discharge, non conducting samples seem to be precluded from analysis, at least in a glow discharge operating in a direct current (dc) mode. Indeed, the latter samples would cause charge buildup as a consequence of ions bombarding the cathode, hereby compensating the applied voltage and thus prohibiting the formation of a plasma. However, this problem can be overcome by applying a radio frequency (rf) voltage to the discharge. Indeed, the more or less continuous positive charge accumulation due to positive ion bombardment will then be neutralized by the large amount of negative charge accumulated by electron bombardment during part of the rf cycle, so that no net charging occurs during the entire rf cycle.

The application of rf power in capacitive coupling to a glow discharge chamber containing two electrodes differing in size, yields a negative dc bias voltage on the smaller electrode surface. Initially, the flux of electrons will exceed the ion flux due to the much higher mobility of the electrons compared to the positive ions. More electrons will be able to reach the larger electrode due to its larger surface area. Since both electrodes are connected to each other by a capacitor in the external circuit, this capacitor will become charged, creating a net negative dc bias voltage on the smaller electrode with respect to the larger electrode. This self-bias phenomenon permits the establishment of a time-averaged cathode and anode in the rf glow discharge, so that sputter-bombardment of positive ions on the cathode, and hence spectroscopic analysis of the cathode material is still possible.

The usefulness of rf glow discharges for analytical spectrochemistry is demonstrated by an increasing number of publications in recent years (*e.g.*, refs. 3–9). Furthermore, for technological purposes, rf glow discharges are far more popular than classical dc glow discharges (*e.g.* refs. 10 and 11).

To improve the capabilities of rf glow discharges, not only for analytical spectrochemistry but also for other application fields, a good understanding of the discharge physics is highly desirable. We attempt to obtain this through mathematical modeling. In the past few years, we have developed a set of models for the various species present in a dc glow discharge in argon, i.e., electrons, argon ions and atoms, excited argon atoms (also in the metastable levels) and sputtered atoms and ions (also in the excited levels) (*e.g.*, refs. 12–22). Now, we would like to extend these models to an rf glow discharge in argon. In the present paper, a model is developed to describe the behavior of electrons and argon ions in an rf glow discharge.

In the literature, different approaches for simulating the behavior of these species are presented. In the so-called *global or analytical models*,[23–25] analytical scaling laws are deduced for the dependence of various plasma quantities on parameters like pressure and rf power. These models are based on some approximations which depend on the specific discharge conditions (*e.g.*, pressure), but they are fast and therefore suitable for a quick prediction of the glow discharge behavior.

Fluid models[26–34] are based on the (first three) velocity moments of the Boltzmann equation, giving rise to a continuity equation, a momentum equation and an energy balance equation. These equations are generally coupled with Poisson's equation, to obtain a self-consistent electric-field distribution. The plasma species are considered as a fluid, a contin-

*E-mail address: bogaerts@uia.ua.ac.be

uum. This type of model is quite fast as well (although it can take considerable time to solve the set of nonlinear, coupled differential equations until convergence), but it is also an approximation. Indeed, it assumes that the velocity distribution functions are almost in equilibrium with the electric field, yet this is not true for fast electrons in the sheath adjacent to the powered rf electrode because they gain more energy from the electric field than they lose by collisions.

Another type of model is based on the full numerical solution of the *Boltzmann equation*.[35] In this case, the nonequilibrium behavior of electrons is taken into account, but the solutions can become mathematically complicated for complex glow discharge geometries.

In *Monte Carlo calculations*,[36–38] the nonequilibrium behavior of the plasma species is also accounted for, but these models are mathematically less complex. Indeed, the plasma species are treated explicitly on the lowest microscopic scale. The trajectory of a large number of particles is calculated by Newton's laws, and their collisions are determined by random numbers and by the collision cross sections. By thus following a large number of particles, the glow discharge can be simulated. However, this model is not self-consistent in the sense that it requires a certain time-dependent electric-field distribution as input, which is clearly a disadvantage. Nevertheless, it can be coupled with Poisson's equation, resulting in a *particle-in-cell (PIC) model*.[39–45] Another disadvantage of this model is that it requires a lengthy computation time because a large number of particles has to be followed to reach satisfactory statistics.

Hence, each model has its advantages and disadvantages. Therefore, a combination of these models is sometimes used, depending on the kind of species to be described. Indeed, species that are far from hydrodynamic equilibrium, like fast electrons, are treated kinetically (*e.g.*, by a Monte Carlo or Boltzmann model), whereas species that can be considered more or less in equilibrium with the electric field, like slow electrons and argon ions, are handled with a fluid model, to save computation time and to obtain self-consistent results (when Poisson's equation is included in the model). This approach is called a *hybrid model*.[46–49] In ref. 50 an excellent overview of all these models, with their specific advantages and disadvantages, is presented for rf glow discharges, and the results of various models have been compared for a specific test case.

In this paper, we present a hybrid model for an argon rf discharge. A Monte Carlo model is used for the electrons, while a fluid model describes both electrons and argon ions. The latter model includes Poisson's equation to calculate the electric field. This field is used as input in the Monte Carlo model, in order to obtain self-consistent results. The present hybrid model is based on our hybrid model for a dc argon glow discharge, presented in refs. 14 and 18. However, there is a significant difference in the treatment of the electrons. In the dc model, the electrons were split up in two groups: the fast electrons were handled with a Monte Carlo method and the slow electrons in the negative glow were followed with a fluid model. In the present rf model, however, both a Monte Carlo and a fluid model are applied for the entire population of electrons, since electrons which are slowed down during one phase of the rf cycle can be accelerated again during the other phase of the cycle, and would therefore have to be described again with the Monte Carlo model. In §2, both the Monte Carlo and the fluid model are discussed, as well as the method of coupling the two models. The results of these models, such as the electrical characteristics (i.e., potential and electrical current), the densities, and the energies and collision rates, are presented in §3. Finally, the conclusions are given in §4.

2. Description of the Model

2.1 Model assumptions

The plasma is assumed to consist of neutral argon gas atoms, thermalized and uniformly distributed throughout the discharge region, electrons and positive argon ions. In reality, a large number of other plasma species are present in the plasma, such as argon atoms in excited levels and fast argon atoms, sputtered atoms and ions. However, these species are only of minor importance in determining the electrical characteristics of the discharge, and are therefore not taken into account in the present model. Nevertheless, in future work, we intend to develop models for these species as well, in analogy to our models for a dc glow discharge.[12–22]

The cell geometry to which the present model is applied, is a simple cylinder with a length of 3 cm and a diameter of 5 mm. All of the cylinder walls are grounded, except for the rf-powered electrode, which is a part of one end of the cylinder. The latter electrode is separated from the grounded cell walls by a 0.1-mm-thick insulating ring. Hence, the rf-powered electrode itself has a diameter of 4.8 mm. This cell is a simplification of the glow discharge source most frequently used for analytical glow discharge optical emission spectrometry (GD-OES), i.e., the LECO GDS 750 (Grimm-type) glow discharge source. Indeed, the latter has a rather complicated geometry with a diameter of 2.5 mm near the rf electrode, which increases gradually to 30 mm at a 10 cm distance from the rf electrode.[51,52] Since the glow discharge plasma is most important in the first few cm's near the rf electrode (based on experimental observations), the cell dimensions assumed for the model are a reasonable approximation. The typical discharge conditions used for rf GD-OES are a gas pressure of 1–10 Torr, discharge power of 5–50 W and an rf frequency of 13.56 MHz. Due to the cylindrical symmetry of the cell geometry under study, the fluid calculations can be performed in two dimensions, i.e., axial (z) and radial (r) directions. The Monte Carlo simulations, however, are carried out in three dimensions.

2.2 Monte Carlo model for electrons

The electrons are followed in time with a Monte Carlo model. Some electrons start at the rf-powered electrode ("secondary electrons"), determined by the flux of argon ions bombarding the rf electrode as a function of time in the rf cycle. The latter is calculated in the fluid model (see below). Hence, the flux of electrons leaving the rf electrode, as a function of time in the rf cycle, is: $j_e(0, r, t) = -\gamma j_i(0, r, t)$, where γ is the ion-induced secondary electron emission coefficient. Further, electrons can also start in the plasma, where they are created by ionization collisions.

The electrons are followed, one after the other, during successive time-steps. Their trajectory is calculated by Newton's laws:

$$z = z_0 + v_{z_0}\Delta t + \frac{qE_{ax}(z, r, t)}{2m}(\Delta t)^2$$
$$x = x_0 + v_{x_0}\Delta t + \frac{qE_{rad}(z, r, t)\cos(\alpha)}{2m}(\Delta t)^2$$
$$y = y_0 + v_{y_0}\Delta t + \frac{qE_{rad}(z, r, t)\sin(\alpha)}{2m}(\Delta t)^2$$
$$v_z = v_{z_0} + \frac{qE_{ax}(z, r, t)}{m}(\Delta t)$$
$$v_x = v_{x_0} + \frac{qE_{rad}(z, r, t)\cos(\alpha)}{m}(\Delta t)$$
$$v_y = v_{y_0} + \frac{qE_{rad}(z, r, t)\sin(\alpha)}{m}(\Delta t) \quad (1)$$

where z_0, x_0, y_0 and z, x, y are the position coordinates before and after Δt, v_{z_0}, v_{x_0}, v_{y_0}, v_z, v_x, v_y are the velocities before and after Δt, E_{ax} and E_{rad} are the axial and radial electric field as a function of axial and radial position and time in the rf cycle (obtained from the fluid model, see below), α is the azimuthal angle of the radial position (i.e. the angle of the radial position coordinates with respect to the x-axis), and q and m are the electron charge and mass, respectively. The probability of collision during one time-step is calculated by

$$Prob_{coll} = 1 - \exp\left(-\Delta s \sum (n\sigma_{coll}(E))\right), \quad (2)$$

where Δs is the distance traveled during Δt; n and $\sigma_{coll}(E)$ are the densities of the target particles and the cross sections of the different collision types of the electron with energy E. This equation is only valid when Δs is small enough so that the densities of the target particles and the electron energy (and hence $\sigma_{coll}(E)$) can be regarded as remaining constant over this distance. In practice, a time-step of 10^{-11} s is used.

A random number between 0 and 1 is generated with a subroutine program, described in ref. 53, and compared with the calculated probability of collision. If the probability is lower than the random number, no collision occurs; if the probability is higher, a collision takes place. The null-collision method was not applied here, because the product of collision cross sections and target particle densities (see eq. (2)) varies so much with energy (i.e., the cross section for electron-electron Coulomb collisions becomes very high at low energies), that a fairly large null-collision cross section would have to be used, and that in most cases (except at very low energy) the collision would be a null-collision anyway.

The collision processes considered in the model are the total electron impact excitation from the argon atom ground state (to all excited levels), electron impact ionization of argon ground state atoms, elastic collisions with argon ground state atoms, and electron-electron Coulomb scattering. Collisions with argon ions are neglected, since these species have a much lower density than argon atoms. The cross sections of the collisions with argon atoms (i.e., excitation, ionization and elastic collisions) as a function of the electron energy, are those reported by Phelps.[54] The following analytical expressions were used to fit the data:[54]

$$\sigma_{exc}(E) = \frac{3.4\times10^{-18}(E-11.5)^{1.1}\left[1+\left(\frac{E}{15}\right)^{2.8}\right]}{1+\left(\frac{E}{23}\right)^{5.5}} + \frac{2.3\times10^{-18}(E-11.5)}{\left(1+\frac{E}{80}\right)^{1.9}}$$
$$\sigma_{ion}(E) = \frac{9.7\times10^{-14}(E-15.8)}{(70+E)^2} + 6\times10^{-18}(E-15.8)^2\exp\left(-\frac{E}{9}\right)$$
$$\sigma_{ela}(E) = 10^{-16}\times\left\{abs\left[\frac{6}{\left(1+\frac{E}{0.1}+\left(\frac{E}{0.6}\right)^2\right)^{3.3}} - \frac{1.1E^{1.4}}{\left[1+\left(\frac{E}{15}\right)^{1.2}\right]\left[1+\left(\frac{E}{5.5}\right)^{2.5}+\left(\frac{E}{60}\right)^{4.1}\right]^{0.5}}\right] + \frac{0.05}{\left(1+\frac{E}{10}\right)^2} + \frac{0.01E^3}{1+\left(\frac{E}{12}\right)^6}\right\} \quad (3)$$

where the cross sections are expressed in cm^2 and the electron energy in eV. Finally, the cross section for electron-electron Coulomb scattering is adopted from[55]

$$\sigma_{e-e}(E_{rel}) = 8\pi b_0^2 \ln\frac{\lambda_D}{b_0}, \quad (4)$$

where E_{rel} is the relative energy of the impacting electron compared to the target electron

$$E_{rel} = E_p + E_t - 2(E_pE_t)^{1/2}\cos\theta, \quad (5)$$

with E_p and E_t being the energy of the projectile and target electron, respectively, and θ being the angle between the velocities of the projectile and target electron (this value is determined by a random number); b_0 is the impact parameter

for a 90° collision (in cm)[55]

$$b_0 = \frac{2.882 \times 10^{-7}}{E_{\rm rel}}, \tag{6}$$

and λ_D is the Debye length (in cm)[56]

$$\lambda_D = \sqrt{\frac{kT_e\varepsilon_0}{n_e e^2}} \tag{7}$$

where k is the Boltzmann constant, ε_0 is the vacuum permittivity, e is the electron charge, and T_e and n_e are the electron temperature and density, respectively. The target electrons are treated as a background gas, as a fluid; their density is obtained from the fluid calculations, whereas their temperature is obtained from the previous Monte Carlo simulation in the iteration procedure (see below).

To determine which type of collision takes place, the fractional probabilities of all the collisions are computed:

$$\begin{aligned}
[n\sigma]_{\rm tot} &= n_{\rm Ar}\sigma_{\rm exc,Ar} + n_{\rm Ar}\sigma_{\rm ion,Ar} + n_{\rm Ar}\sigma_{\rm ela,Ar} + n_e\sigma_{e-e} \\
P_{\rm exc,Ar} &= \frac{n_{\rm Ar}\sigma_{\rm exc,Ar}}{[n\sigma]_{\rm tot}} \cdot P_{\rm ion,Ar} = \frac{n_{\rm Ar}\sigma_{\rm ion,Ar}}{[n\sigma]_{\rm tot}} \\
P_{\rm ela,Ar} &= \frac{n_{\rm Ar}\sigma_{\rm ela,Ar}}{[n\sigma]_{\rm tot}} \cdot P_{e-e} = \frac{n_e\sigma_{e-e}}{[n\sigma]_{\rm tot}}
\end{aligned} \tag{8}$$

The sum of the fractional probabilities is equal to unity, and the interval [0, 1] is divided into segments with lengths corresponding to these fractional probabilities. A new random number between 0 and 1 is generated, and the interval into which this random number falls, determines the type of collision that occurs. The new energy and direction after the collision depends upon the type of collision: For *excitation*, the new energy E is given by: $E = E_0 - E_{\rm exc}$, where $E_{\rm exc}$ is the excitation threshold energy (i.e., taken as 11.55 eV for excitation from the argon ground state), and E_0 is the electron energy before collision. For *ionization*, the total energy before collision is divided between the primary (original) electron and the secondary electron created in the ionization collision, using a random number (RN). The energy of the primary electron ($E_{\rm prim}$) after the collision is defined by[57]

$$RN = \frac{\displaystyle\int_0^{E_{\rm prime}} \sigma_{\rm ion,diff}(E_0, \varepsilon)d\varepsilon}{\sigma_{\rm ion}(E_0)}, \tag{9}$$

where $\sigma_{\rm ion,diff}(E_0, \varepsilon)$ and $\sigma_{\rm ion}(E_0)$ are the differential ionization cross section to create a primary electron with energy ε (adopted from ref. 58) and the total ionization cross section, respectively, E_0 is the energy before collision and ε is the energy of the primary electron after collision. The energy of the secondary electron after the collision is then given by: $E_{\rm sec} = E_0 - E_{\rm ion} - E_{\rm prime}$, where $E_{\rm ion}$ is the ionization threshold energy (i.e., 15.76 eV) and the other symbols remain as explained above. For *elastic collisions*, the new kinetic energy of the electron is calculated by[59]

$$E = E_0\left[1 - 2\frac{m_e}{m_{\rm Ar}}(1 - \cos\chi)\right], \tag{10}$$

which is deduced from the hard-sphere model. χ is the scattering angle of the electron after collision (see below). For all three types of collisions with argon atoms, the new direction after collision is determined by anisotropic scattering.[60] The scattering angle χ and the azimuthal angle of scattering ψ are defined by two random numbers:[60]

$$\begin{aligned}
RN &= \frac{2\pi}{\sigma(E_0)}\int_0^{\chi} \sigma(E_0, \chi')\sin\chi' d\chi' \\
\psi &= 2\pi RN
\end{aligned} \tag{11}$$

where $\sigma(E_0)$ is the total cross section of a particular collision and $\sigma(E_0, \chi)$ is the angular differential cross section, adopted from ref. 60. Substituting the analytical expression of $\sigma(E_0, \chi)/\sigma(E_0)$[60] into the integral, and solving it analytically, yields

$$\chi = 2\arcsin\sqrt{\frac{\exp[RN\ln(1 + E_0)] - 1}{E_0}}. \tag{12}$$

The scattering angle of the secondary electron in an ionization collision is determined from the law of conservation of momentum, and is therefore fixed by the direction of the primary electron. The parameters of this secondary electron (coordinates, energy, direction) are stored in an array, so that this electron can be followed as well from the next time-step.

Finally, for electron-electron Coulomb scattering, isotropic scattering is assumed,[61] and χ and ψ are calculated as

$$\begin{aligned}
\chi &= 2\arccos(RN), \\
\psi &= 2\pi RN.
\end{aligned} \tag{13}$$

The energy loss (if the energy of the projectile electron (E_p) is higher than the energy of the target electrons (E_t)), or the energy gain (if $E_p < E_t$) is computed as[61]

$$\Delta E = \begin{cases} E_p(1 + \cos\chi)/2 & \text{(Loss if } E_p > E_t\text{)} \\ E_t(1 + \cos\chi)/2 & \text{(Gain if } E_p < E_t\text{)}. \end{cases} \tag{14}$$

The new three-dimensional direction after collision (defined by the axial and azimuthal angles θ and ϕ) can now be calculated from the axial and azimuthal angles of scattering, χ and ψ, and from the axial and azimuthal angles before collision, θ_0 and ϕ_0, by transformation of the coordinate frame of reference:[14]

$$\begin{pmatrix} \sin(\theta)\cos(\phi) \\ \sin(\theta)\sin(\phi) \\ \cos(\theta) \end{pmatrix} = \begin{pmatrix} \cos(\theta_0)\cos(\phi_0) & -\sin(\phi_0) & \sin(\theta_0)\cos(\phi_0) \\ \cos(\theta_0)\sin(\phi_0) & \cos(\phi_0) & \sin(\theta_0)\sin(\phi_0) \\ -\sin(\theta_0) & 0 & \cos(\theta_0) \end{pmatrix} \times \begin{pmatrix} \sin(\chi)\cos(\psi) \\ \sin(\chi)\sin(\psi) \\ \cos(\chi) \end{pmatrix} \tag{15}$$

When the new energy and three-dimensional direction after collision are calculated, the coordinates (x, y and z), the energy and the three-dimensional direction (θ and ϕ) of this electron are stored in an array, and the next electron is followed during that time-step in the same way (i.e., calculation of the trajectory by Newton's laws, determination and treatment of the collisions by random numbers, and storage of the electron parameters). When all electrons have been followed, we move to the next time-step, to follow all the electrons again, i.e., the electrons stored after following during the previous time-step, the electrons created by ionization collisions in the previous time-step, as well as the new electrons starting

at the rf electrode (determined by the ion flux bombarding the electrode as a function of time in the rf cycle).

However, it may also be possible that some electrons are removed from the Monte Carlo procedure when they collide with the cell walls. Indeed, they can be absorbed, reflected or cause secondary electron emission. Tantalum is used in this model simulation as the cell-wall material. The secondary electron emission coefficient for tantalum, δ, as a function of the electron energy, is taken from ref. 62 and is rather high (i.e., maximum 1.3 at 600 eV), which means that electrons of considerable energy easily cause the emission of a secondary electron. When δ is higher than 1, at least one secondary electron is emitted, which is also stored in the array and followed from the next time-step. Moreover, the calculated value of δ (if $\delta < 1$) or of $\delta - 1$(if $\delta > 1$) is compared with a RN between 0 and 1. If δ(or $\delta - 1$) $< RN$, no (extra) secondary electron emission takes place and the electron is simply absorbed by the cell walls. If δ(or $\delta - 1$) $> RN$, (an additional) secondary electron emission has taken place. It is assumed that about 10% of the electrons are emitted as primary electrons (i.e., they are just specularly reflected with no change in energy), whereas the remaining 90% are emitted as secondary electrons, with energies of 4 eV and in a direction randomly chosen with respect to the normal of the wall.[63]

This entire procedure of following all electrons during successive time-steps is repeated over a number of rf cycles, until the periodic steady-state is reached, i.e., when the results cease to change from one rf cycle to the next. The final calculation results, such as electron density, flux, energy, collision frequency, etc., are only computed in the last rf cycle followed. In practice, it was found that, for the discharge conditions under investigation (i.e., $p = 6$ Torr, $P = 10$ W), the complete steady-state is already reached at 2 rf cycles (see Figs. 9 and 10). This follows also from simple estimations about the time necessary for the thermalization of the electrons. The cross section of ionization collisions is typically 10^{-16} cm^2. The density of argon gas atoms at 6 Torr is of the order of 10^{17} cm^{-3}. Hence, an electron with energy of 100 eV (corresponding to a velocity of 6×10^8 cm/s) undergoes approximately 6×10^9 collisions per second, which means approximately 450 collisions per rf cycle ($T_{rf\,cycle} = 7.4 \times 10^{-8}$ s). Suppose that the electron loses approximately 16 eV in an ionization collision, only 6–7 ionization collisions would be required to thermalize an electron with 100 eV initial energy. Of course, the electrons can also gain energy during some part of the rf cycle, but this simple calculation shows that most electrons will be thermalized within one rf cycle and will not play a major role in any subsequent rf cycles. Based on comparisons of the calculation results for various numbers of rf cycles, we decided to follow the electrons during 2 rf cycles.

It is clear that this method of calculation requires a long computation time. Indeed, in our previous dc model,[14] the electrons were transferred to the fluid model when they reached energies below the excitation threshold, whereas in the present rf model, all electrons are simulated by the Monte Carlo method. Since slow electrons will stay in the plasma for a very long time, a method is developed to combine these electrons into a "superelectron" with a larger weight factor, based on the procedure described in ref. 64, in order to decrease the computation time. If the electrons in the bulk plasma have energies below a certain threshold (taken as 1 eV in this study), a fraction defined by "ftoss", will be removed from the Monte Carlo model. Therefore, a RN between 0 and 1 is generated. If $ftoss > RN$, the electron is removed. If $ftoss < RN$, the electron remains in the model, and since the real number of slow electrons must be constant, there must be compensation for those which disappear; hence, the weight of those which remain is increased by: $w = w/(1 - ftoss)$. This clearly indicates that a larger value for ftoss will result in a more efficient reduction in computation time, but on the other hand, a too large value will affect the statistics of the Monte Carlo model. In practice, we found that a value equal to 0.5 yielded satisfactory and statistically valid results within a reasonable computation time.

2.3 *Fluid model for the argon ions and electrons*

Besides the Monte Carlo model, the electrons are also treated in a fluid model, together with the argon ions. The equations are the first three velocity moments of the Boltzmann equation, i.e., the balance equations for particle density, for momentum density and for energy density.

Particle density balance equations

$$\frac{\partial n_{Ar^+}(z,r,t)}{\partial t} + \overline{\nabla} \cdot \overline{j_{Ar^+}}(z,r,t) = R_{Ar^+}(z,r,t). \tag{16}$$

$$\frac{\partial n_e(z,r,t)}{\partial t} + \overline{\nabla} \cdot \overline{j_e}(z,r,t) = R_e(z,r,t). \tag{17}$$

where n_{Ar} and n_e are the argon ion and electron densities, $\overline{j_{Ar^+}}$ and $\overline{j_e}$ are the corresponding fluxes (in vector notation), and R_{Ar^+} and R_e are the creation rates of argon ions and electrons, which result from the Monte Carlo model (i.e., $R_{Ar^+} = R_e =$ the rates of electron impact ionization; see below).

Momentum balance equations

At the pressure under investigation here (i.e., 6 Torr), the characteristic time interval between momentum transfer collisions is much smaller than the rf period, and the mean free path for these collisions is much smaller than the characteristic lengths in the discharge. Therefore, the momentum balance equations for argon ions and electrons can be reduced to the flux equations based on diffusion and on migration in the electric field, as explained in ref. 65.

$$\begin{aligned}\overline{j_{Ar^+}}(z,r,t) =& \mu_{Ar^+} n_{Ar^+}(z,r,t) \overline{E}^{\,\mathrm{eff}}(z,r,t) \\ & - D_{Ar^+} \overline{\nabla} n_{Ar^+}(z,r,t).\end{aligned} \tag{18}$$

$$\begin{aligned}\overline{j_e}(z,r,t) =& -\mu_e n_e(z,r,t) \overline{E}(z,r,t) \\ & - D_e \overline{\nabla} n_e(z,r,t).\end{aligned} \tag{19}$$

where $\overline{E}$ is the electric field; since the argon ions cannot follow the fluctuating rf electric field, they are assumed to be in an effective field, $\overline{E}^{\,\mathrm{eff}}$, which is determined from:[65]

$$\frac{\partial \overline{E}^{\,\mathrm{eff}}(z,r,t)}{\partial t} = \nu_m \left(\overline{E} - \overline{E}^{\,\mathrm{eff}} \right). \tag{20}$$

where ν_m is the ion momentum-transfer frequency,

$$\nu_m = \frac{e}{\mu_{Ar^+} m_{Ar^+}}, \tag{21}$$

where D_{Ar^+}, D_e, μ_{Ar^+} and μ_e are the argon ion and electron diffusion coefficients and mobilities, respectively. Their numerical values are taken to be:[32] $D_{Ar^+} = 40\,\mathrm{cm^2\,s^{-1}}$,

$D_e = 1.2 \times 10^6\ \mathrm{cm^2\ s^{-1}}$, $\mu_e = 3 \times 10^5\ \mathrm{cm^2\ s^{-1}\ V^{-1}}$, $\mu_{Ar^+} = 1500\ \mathrm{cm^2\ s^{-1}\ V^{-1}}$ at 1 Torr and 298 K. Finally, e and m_{Ar^+} are the electronic charge and mass of the argon ion, respectively.

Energy balance equations

The argon ions are assumed to have thermal energies, constant in time and space, because they exchange their energy very efficiently with the background argon gas. Therefore, no energy equation is used for the argon ions. The electron energy balance equation is written as[32]

$$\frac{\partial w_e(z,r,t)}{\partial t} + \overline{\nabla}\cdot\left(\frac{5}{3}\varepsilon_e(z,r,t)\overline{j_e}(z,r,t) + \overline{q}(z,r,t)\right) = -e\overline{j_e}(z,r,t)\cdot\overline{E}(z,r,t) - R_{w,e}(z,r,t), \tag{22}$$

where w_e is the electron energy density given by: $w_e = n_e\varepsilon_e$, where ε_e is the electron energy. The second term of the left-hand side, between the brackets, describes the energy transport: $\overline{j_e}$ is the electron flux, given by diffusion and migration (see eq. (19) above), and $\overline{q}$ is the heat flux:

$$\overline{q}(z,r,t) = -\frac{2}{3}\kappa\overline{\nabla}\varepsilon(z,r,t), \tag{23}$$

where κ is the thermal conduction coefficient, given by: $\kappa = 5/2 n_e D_e$. Substituting the formulas for $\overline{j_e}$ and $\overline{q}$ in the term between the brackets, and combining the terms, yields

$$\frac{\partial w_e(z,r,t)}{\partial t} + \overline{\nabla}\cdot\left(-\frac{5}{3}\mu_e w_e(z,r,t)\overline{E}(z,r,t) - \frac{5}{3}D_e\overline{\nabla}w_e(z,r,t)\right) = -e\overline{j_e}(z,r,t)\cdot\overline{E}(z,r,t) - R_{w,e}(z,r,t), \tag{24}$$

The first term on the right-hand side describes the energy gain by the electric field (i.e., Ohmic heating, $\overline{E}$ is the electric field), and the second term, $R_{w,e}$, gives the electron energy loss due to collisions (i.e., electron impact ionization rate multiplied by the ionization energy + electron impact excitation rate multiplied by the excitation energy, both obtained from the Monte Carlo model; energy losses due to elastic collisions with argon atoms can be neglected due to the large mass difference).

Poisson's equation

Finally, the equations are coupled with Poisson's equation to obtain a self-consistent potential and electric-field distribution:

$$\nabla^2 V(z,r,t) + \frac{e}{\varepsilon_0}\left(n_{Ar^+}(z,r,t) - n_e(z,r,t)\right) = 0 : \overline{E} = -\overline{\nabla}V, \tag{25}$$

where ε_0 is the permittivity in vacuum.

The flux equations (eqs. (18) and (19) can be substituted into eqs. (16) and (17). This leads to a set of four coupled differential equations, i.e., the continuity equations for argon ions and electrons (eqs. (16) and (17)), the energy balance equation for electrons (eq. (24)) and Poisson's equation for the electric field (eq. (25)). The boundary conditions for these equations are taken as follows:

- At the rf electrode: $V(t) = V_{dc} + V_{rf}\sin(\omega_{rf}t)$, where ω_{rf} is the rf frequency, V_{rf} is the applied rf voltage and V_{dc} is the autobias voltage developed at the rf electrode (see below).
- At the grounded cell walls: $V(t) = 0$.
- $n_e = 0$ at all walls at all times because electron recombination at a conducting surface is assumed to be infinitely fast.
- $w_e = 0$ at all walls at all times because $w_e = n_e\varepsilon_e$ (see above).
- $\overline{\nabla}n_{Ar^+} = 0$ at all walls at all times. This means that the ion flux at the walls is only due to migration.

The boundary conditions for the densities are not exact. In fact, they should be replaced by a mixed boundary condition because electrons and ions recombine at the walls.[66] However, this would hardly influence the resultant density profiles because the electric field is high and points toward the walls.

Due to the severe nonlinearity and strong coupling of the equations, solving this model is a difficult numerical problem. The method we used was developed by Goedheer and coworkers.[29,32,65] It is a fully implicit method, based on the Scharfetter-Gummel exponential scheme for the transport equations.[26,29,32,65,67,68] The basic idea is that the particle fluxes are assumed to be constant between mesh points, instead of the densities. The advantage of this scheme is its ability to switch between situations where either the migration component or the diffusion component of the particle flux is dominant (i.e. high and low electric field, sheath region and bulk plasma, respectively). More details about the Scharfetter-Gummel scheme can be found in refs. 14, 29 and 32.

After discretization, the four equations (i.e., ion continuity, electron continuity, electron energy, and Poisson's equation) are solved as a function of time. Because of the high mobility of the electrons, fully implicit handling is necessary for the electron continuity equation. Therefore, the latter equation is solved simultaneously with Poisson's equation for the self-consistent electric field at each time-step, using the Newton-Raphson method. Solving both electron continuity and Poisson's equations with this method at each z and r position leads to a large bi-tridiagonal matrix (the Jacobian), which could be converted into a pentadiagonal matrix and solved by elimination of rows. After n_e and V are known, the discretized electron energy equation is solved to obtain w_e at all z and r positions (i.e., a tridiagonal matrix). Finally, the ion continuity equation is solved (also a tridiagonal matrix) using the known values of V at that time-step. When the values for all four variables at each z and r position are known at time $k+1$, the procedure is repeated for time $k+2$, etc., until the steady state is reached in the periodic solution (i.e., when all variables at all z and r positions have the same value at the beginning and at the end of the rf cycle). In practice, we performed the calculations in a cylindrical region on a nonequidistant grid with 64 cells in the z-direction and 32 cells in the r-direction. Furthermore, 256 time-steps were considered within one rf cycle.

The input parameters in the fluid model are the geometry, the boundary conditions, the pressure and the discharge power, as well as the creation rates for ions and electrons and the energy-loss rate for the electrons, both obtained from the Monte Carlo model. Moreover, an initial estimate is made for the rf and dc bias voltages, V_{rf} and V_{dc}. As explained above, besides the rf voltage, a negative dc bias voltage is present in the case of two capacitively coupled electrodes of different sizes. It is due to the much lower mass, and hence higher

mobility, of the electrons compared to the ions. It arises to repel the electrons and attract the ions, until the steady state is reached and the total flux of electrons reaching the rf electrode during the entire rf cycle is equal to the total flux of ions (see above, in the introduction). Since we are only interested in the final quasi steady state, the circuit equations are not solved in our model, but the initial dc bias is adapted after each rf cycle by the condition that the total electron flux at the rf electrode, integrated over the entire rf cycle must be equal to the total ion flux.[69] In practice, during each rf cycle, the total electron and ion fluxes at the rf electrode are calculated. If the electron flux is higher, the value of V_{dc} is lowered by a certain step (i.e., defined by the difference in total electron and ion fluxes); if the electron flux is lower, V_{dc} is increased until both fluxes are equal to each other within a certain accuracy. In fact, in this way, an infinitely large coupling capacitor is simulated.

In a similar way, the initial value of V_{rf} is also adapted after each rf cycle. Indeed, the amount of power dissipated by electrons and ions, integrated over the entire discharge region and rf cycle is calculated (i.e., the energy gain of ions and electrons due to the electric field, by Ohmic heating), and compared with the fixed power input into the system. If the power dissipated by electrons and ions is lower (or higher) than the input power, then the value of V_{rf} is increased (or decreased) by a certain amount (again defined by the difference in dissipated and input power), until they are equal within the required accuracy.

2.4 *Coupling procedure*

The Monte Carlo and fluid models are run iteratively, until convergence is reached. First, the fluid equations are solved, assuming arbitrary values for the ion and electron production rate and for the electron energy loss due to collisions. The results of this fluid model are the electric field as a function of (axial and radial) position and time in the rf cycle, as well as the ion flux bombarding the rf electrode, as a function of radial position and time in the rf cycle. These values are used in the Monte Carlo model, i.e., the electric field determines the trajectory of the electrons, and the ion flux bombarding the rf electrode defines the electron flux leaving the rf electrode as a function of radial distance and of time in the rf cycle. Moreover, the electron density is also adopted from the fluid model, to be used in electron-electron Coulomb collisions (see above). The Monte Carlo model yields, among others, the number of ionization and excitation collisions carried out by the electrons, which are used as source terms in the fluid model. The ionization collisions determine the creation rate of ion-electron pairs, whereas both ionization and excitation collisions, multiplied with the energy loss during such collision, define the energy loss for the electrons, used in the electron energy balance equation. With the new source terms, the fluid equations are again solved, etc. The procedure is repeated until convergence is reached, i.e., when V_{dc}, V_{rf} and the total ion flux bombarding the rf electrode do not change anymore. This is typically the case after three-seven iterations, depending on the choice of the initial conditions.

The calculations are performed on a Digital Personal Workstation, at a clock speed of 433 MHz (DPW433 au) and approximately 1 GB RAM. The Monte Carlo model requires a few hours of calculation time when 100,000 electrons starting at the rf electrode (integrated over the two rf cycles to be followed) are simulated, together with all the electrons that are created in ionization collisions. The fluid model usually takes about one night before complete convergence is reached (i.e., when the relative errors in the densities, potential and electron energy are smaller than *e.g.*, 10^{-5}). However, the succession of Monte Carlo and fluid models is performed more rapidly, when intermediate convergence is reached (i.e., when V_{dc} and V_{rf}, and, hence, the electric field, stay more or less constant), and occurs after only a few hours computation time (or several hundreds rf cycles in the program). Nevertheless, the entire calculation procedure of the hybrid model may require several days.

3. Results and Discussion

3.1 *Electrical characteristics*

The calculations are performed at discharge conditions typical for rf glow discharges used in optical emission spectrometry (rf GD-OES), i.e., the rf frequency is 13.56 MHz, a power of 10 W is chosen and the gas pressure is 6 Torr. Since the glow discharge chamber has a rather small volume (i.e., length of 3 cm and diameter of 5 mm), it is expected that the amplitude of the rf voltage (V_{rf}) will have to be quite high in order to dissipate the input power of 10 W (see above). Moreover, the rf-powered electrode (which forms one end of the cell) is much smaller than the grounded electrode (which is given by the other cell walls); hence, the dc bias voltage (V_{dc}) is also expected to be rather high. Indeed, after complete convergence of the hybrid model, we calculated that V_{rf} is 900 V and V_{dc} is -610 V at the discharge conditions under study.

Figure 1 shows the calculated potential at the rf electrode during an rf cycle, when the periodic "steady state" is reached ($V_{rf\,electrode}$: solid line). It is only positive during one quarter of the rf cycle (i.e., ωt ranging from approximately $\pi/4$ to approximately $3\pi/4$). Moreover, it is extremely negative around $\omega t = 3\pi/2$, i.e., equal to the sum of V_{dc} and V_{rf}. This highly negative value gives rise to a high electric field near the rf electrode. Hence, the ions will be accelerated towards the rf electrode, and cause a large amount of sputtering, which is of great importance for glow discharges used in analytical chemistry.

The calculated values of V_{rf} and V_{dc} cannot be directly

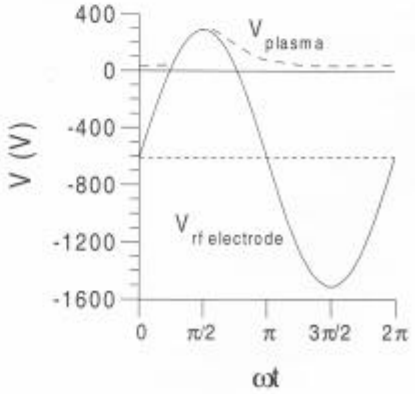

Fig. 1. Potential at the rf electrode ($V_{rf\text{-}electrode}$: solid line) and plasma potential (V_{plasma}: dashed line), as a function of time in the rf cycle ($p = 6$ Torr, $P = 10$ W).

compared with experimental data, since the cell under consideration here is a simplification of the real rf glow discharge source used for OES. Nevertheless, the obtained values are comparable to typical measured values,[52] so that we can consider that our calculations present a realistic picture of the rf glow discharges used for rf GD-OES.

Figure 1 illustrates also the calculated plasma potential as a function of time in the rf cycle (V_{plasma}; dashed line). This value is always positive, as in the dc case, but oscillates between a minimum and a maximum value and is strongly anharmonic. It is highest when the potential at the rf electrode is positive (around $\omega t = \pi/2$, $V_{plasma} = V_{rf\text{-}electrode}$), and reaches its minimum when $V_{rf\text{-}electrode}$ is most negative ($\omega t = 3\pi/2$). However, the time evolution of V_{plasma} shows a slight delay with respect to $V_{rf\text{-}electrode}$. Indeed, the maximum value is obtained sometime after the maximal $V_{rf\text{-}electrode}$ is obtained and decreases less rapidly, so that the value at $\omega t = \pi$ is slightly higher than the values at $\omega t = 0 = 2\pi$, whereas the values of $V_{rf\text{-}electrode}$ are the same at $\omega t = 0$, π and 2π.

Figure 2 shows the two-dimensional potential distribution (in cylindrical symmetry) at four different times in the rf cycle. At $\omega t = \pi/2$ the potential is positive and rather high throughout the entire discharge region, reaching +290 V at the rf electrode. Indeed, the largest electrode is now the momentary cathode, and since the latter is grounded, the rest of the plasma must be positive. At $\omega t = \pi$, $3\pi/2$ and 2π, the potential distribution is comparable to the dc case. Indeed, it is extremely negative at the rf electrode (the "cathode"), i.e., −610 V at $\omega t = \pi$ and 2π, and −1510 V at $\omega t = 3\pi/2$. It increases rapidly in the sheath, crosses zero at somewhat less than 1 mm from the rf electrode, and is positive in the rest of the plasma. The plasma potential (defined here as the maximum value in the plasma) varies between approximately 30 V at $3\pi/2$ and approximately 290 V at $\omega t = \pi/2$, as was illustrated in Fig. 1. Moreover, as was also anticipated from Fig. 1, the potential distributions at $\omega t = \pi$ and 2π are not exactly equal to each other.

The position where the potential crosses zero is defined here as the boundary between the rf sheath and the bulk plasma. This definition is not precise; for example, it cannot be applied to define a sheath at the grounded electrode, since the potential is zero at the electrode itself. In reality, the subdivision between the sheath and bulk is somewhat arbitrary. It can, for example, also be defined as the position where the positive ion and electron densities become equal to each other, or more precisely, the position where the ions reach a velocity larger than $(kT_e/m_i)^{1/2}$ towards the electrode (i.e., Bohm sheath criterion).[56] However, the definition of the potential crossing the zero-line is the simplest and most straightforward, and is therefore used here. Figure 3 presents the thickness of the rf sheath at the cell axis as a function of time in the rf cycle. Generally, its value is less than 1 mm, as demonstrated in Fig. 2. The rf sheath is thickest at $\omega t = 3pi/2$, since the largest potential has to drop off. Moreover, it is zero from $\omega t = \pi/4$ to $3\pi/4$, when the rf electrode is positive and no sheath is formed in front of it. Hence, in contrast to the dc case, the sheath moves towards and away from the rf electrode.

This moving of the sheath gives rise to a change in the accumulated positive charge in the sheath. Since $I = dq/dt$, the latter gives rise to a current, called "displacement current", which is expressed as[65]

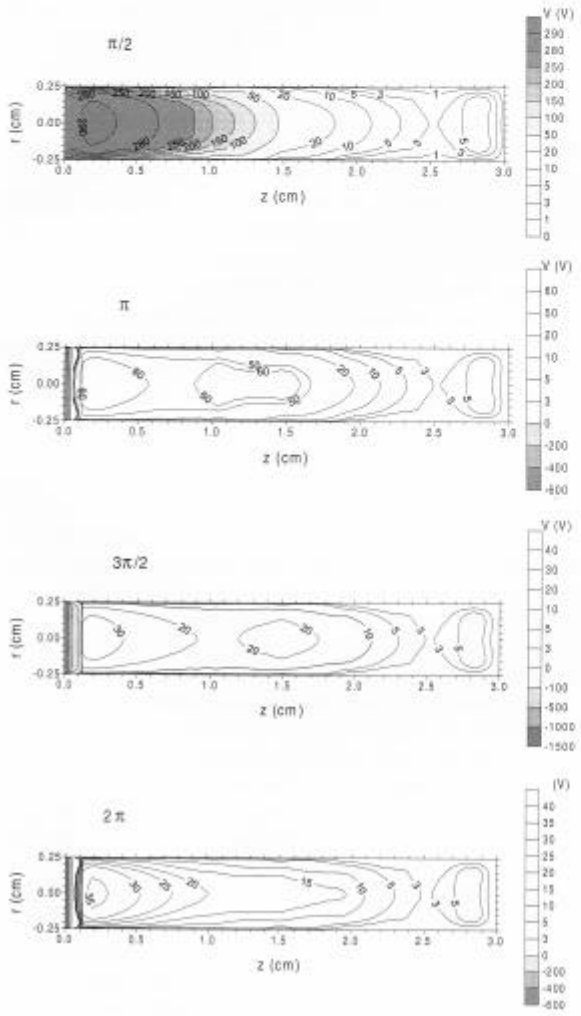

Fig. 2. Two-dimensional potential distribution throughout the discharge, at four times in the rf cycle ($p = 6$ Torr, $P = 10$ W).

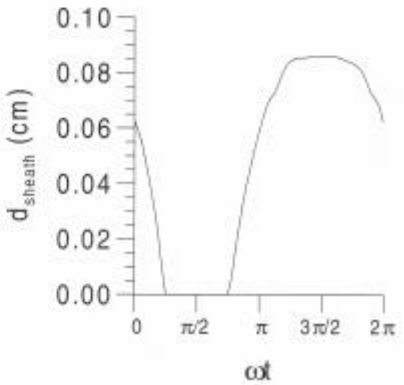

Fig. 3. Thickness of the rf sheath (d_{sheath}) as a function of time in the rf cycle ($p = 6$ Torr, $P = 10$ W).

$$J_D = \varepsilon_0 \frac{\partial E}{\partial t},$$

where ε_0 is the permittivity in vacuum. Indeed, the rf sheath is characterized by a positive space charge (see below). Since the rf sheath changes its thickness during the rf cycle and the argon-ion density value remains constant (see below), the total positive space charge in the sheath changes accordingly. Therefore, the total rf current flowing through the discharge cell is the sum of the ion current, electron current and displacement current:

$$J_{total} = eJ_i - eJ_e + J_D$$

The total current at the rf-powered electrode as a function of time in the rf cycle, and the various contributions, are illustrated in Fig. 4 (a negative sign denotes a flux in the negative z-direction, hence towards the rf electrode). The ion flux (J_i) is always directed towards the rf electrode, and during a large part of the rf cycle, it contributes predominantly to the total current to the rf electrode (J_{total}). However, during the part when the rf electrode is positive, a high electron flux (J_e) is directed towards the rf electrode, and the electrical current to the rf electrode is then almost exclusively due to the electrons. It can be observed that the displacement current is almost negligible at the discharge conditions under investigation (i.e., it varies between +0.025 and −0.025 mA). Indeed, this current is typical for rf discharges with electrodes of comparable size, when the rf sheaths change considerably. Since the glow discharge cell under consideration gives rise to a large dc bias, so that the positive ion sheath is present most of the time in front of the rf electrode, it resembles a dc glow discharge, where the displacement current is absent. The total electrical current, integrated over the entire rf cycle, is zero, which is imposed by the capacitive coupling (see above).

3.2 *Positive ion and electron densities*

Figure 5 illustrates the two-dimensional argon-ion density profile. It is constant throughout the rf cycle, since the ions cannot follow the rapidly fluctuating electric field, they are assumed to be only in an "effective field" (see above), which is nearly equal to the time-averaged field. The density profile resembles the dc argon-ion density distribution: it is low and rather constant in the sheath (approximately 10^{11} cm^{-3}), increases to a maximum of approximately 5×10^{12} cm^{-3} at about 2 mm from the cathode (i.e., in the beginning of the bulk plasma), and decreases again towards the cell walls. In a dc glow discharge used for analytical purposes, ion density values on the order of 10^{11}–10^{13} cm^{-3} were calculated,[14,18,70] depending on the discharge conditions. In a future work, we plan to perform a detailed comparison between dc and rf discharges, to investigate which operation mode yields the highest plasma density under similar conditions of pressure and power.

The electron density has a similar profile as the ion density. The maximum is also approximately 5×10^{12} cm^{-3}, at the same position in the plasma, but the electron density is different near the rf electrode. At $\omega t = \pi/2$, the electron density in the sheath is approximately equal to the argon-ion density and has a more or less constant value of 10^{11} cm^{-3}. However, at $\omega t = 3\pi/2$ the electron density decreases rapidly to zero in the rf sheath, giving rise to a positive space charge and hence, a large potential drop (as was shown in Fig. 2). Between these two extremes, at $\omega t = \pi$ and $\omega t = 2\pi$, the electron density decreases to a zero value towards the rf electrode, but less rapidly than at $\omega t = 3\pi/2$, giving rise to a thinner rf sheath in front of the rf electrode (see Fig. 2).

3.3 *Mean electron energy*

The mean electron energies as a function of distance from the rf electrode, calculated at four different times in the rf cycle, are depicted in Fig. 6. The electron energy was always taken to be equal to 4 eV at the rf electrode. At $\omega t = 3\pi/2$, it increases rapidly to a maximum of approximately 640 eV at 0.05–0.1 cm from the rf electrode. Since the total voltage drop over the rf sheath is equal to 1510 V in this case (see above), the mean electron energy is, at maximum, about 40% of the total voltage drop. The mean electron energy decreases again before the interface between the rf sheath and the bulk plasma is reached, because the electrons will now lose more energy by collisions than they gain from the (lower) rf electric field. In the bulk plasma, the mean electron energy varies between 50 and 90 eV in the first 2 cms from the rf electrode, and drops to low values (1–5 eV) still further away.

Also at $\omega t = \pi$ and 2π, the mean electron energy reaches a maximum in the rf sheath. The maximum value is about 220–250 eV, which is about 40% of the total sheath voltage drop at that time. In the plasma bulk, typical values of about 10–30 eV were calculated, decreasing again to a few eV after moving further than 1 cm from the rf electrode. At $\omega t = \pi/2$, the mean electron energy was calculated to be about 3–5 eV

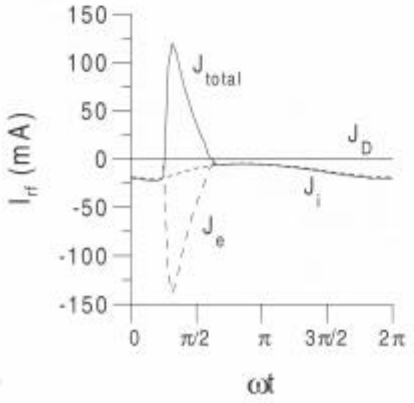

Fig. 4. Total electrical current at the rf electrode (J_{total}), and contributions of the ion flux (J_i), electron flux (J_e) and displacement current (J_D) at the rf electrode, as a function of time in the rf cycle ($p = 6$ Torr, $P = 10$ W).

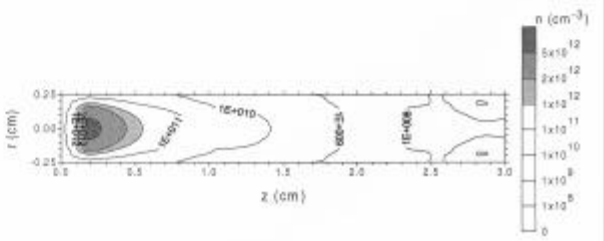

Fig. 5. Two-dimensional argon-ion density profile throughout the discharge (constant during the entire rf cycle) ($p = 6$ Torr, $P = 10$ W).

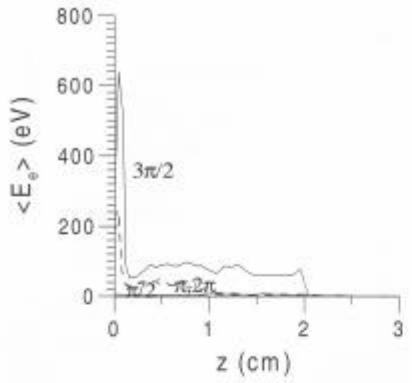

Fig. 6. Mean electron energies as a function of distance from the rf electrode, at four times in the rf cycle ($p = 6$ Torr, $P = 10$ W).

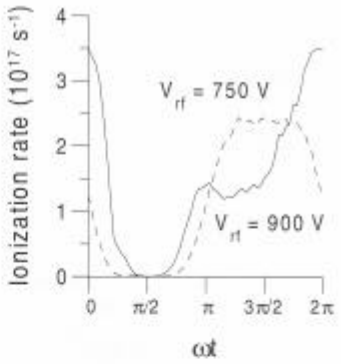

Fig. 7. Total electron impact ionization rate, integrated over the entire discharge volume, as a function of time in the rf cycle (solid line: $p = 6$ Torr, $P = 10$ W, $V_{rf} = 900$ V). For comparison, the results at a lower rf voltage (i.e., $V_{rf} = 750$ V) are also denoted by the dashed line.

throughout the entire discharge region.

The results presented in Fig. 6 were obtained with the Monte Carlo model, but the same quantities have been calculated with the fluid model. In the bulk plasma, the results of both models agreed quite well, but in the rf sheath, some discrepancies were observed for $\omega t = \pi$, $3\pi/2$ and 2π. This is not completely unexpected, since the electron density at these times in the rf cycle is very low, and the calculated energy in the fluid model is also not very reliable. Moreover, at the high electric field present at these times in the rf sheath, the approximation in the fluid model of nearly hydrodynamic equilibrium for the electrons is not actually valid. However, at $\omega t = \pi/2$, both the Monte Carlo and the fluid model predict comparable mean electron energies, which shows that the fluid model gives a reasonable approximation at this phase of the rf cycle.

3.4 *Collision rates*

Figure 7 shows the total argon-ionization rate, integrated over the entire discharge volume, as a function of time in the rf cycle. It appears that the ionization is at its maximum around $\omega t = 2\pi$, and very low around $\omega t = \pi/2$. The latter was expected, since at this time in the rf cycle, the mean electron energy is on the order of 3–5 eV (see Fig. 6), and only a limited fraction of the electrons has enough energy to cause ionization. At $\omega t = 3\pi/2$, the mean electron energy is very high, but it appears to be too high for efficient ionization. Indeed, the maximum in the cross section for electron impact ionization is around 100 eV, and electrons with higher energy will therefore cause less ionization. The same effect was also observed in a dc glow discharge.[16] Therefore, it appears that, under the present discharge conditions, the most efficient ionization takes place around $\omega t = 2\pi$. It should be mentioned, however, that this result cannot be generalized, and applies only to the discharge conditions under study (i.e., high rf and dc bias voltages). Indeed, we have found that at somewhat lower voltages (*e.g.*, $V_{rf} \sim 750$ V and $V_{dc} \sim -500$ V), the most efficient ionization occurs at $\omega t = 3\pi/2$, as is illustrated in Fig. 7 (dashed line).

The same time evolution was also observed for the other collision rates calculated with the Monte Carlo model (i.e., excitation, elastic and electron-electron Coulomb collisions), because more ionization collisions give rise to more electrons, which can in turn produce more collisions.

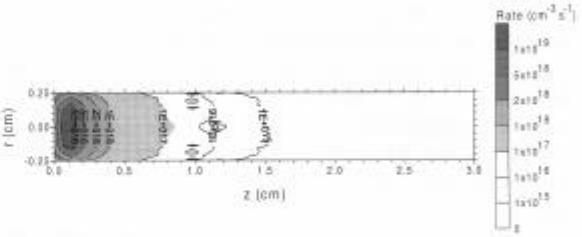

Fig. 8. Two-dimensional ionization rate profile throughout the discharge, at $\omega t = 2\pi$ ($p = 6$ Torr, $P = 10$ W).

The two-dimensional ionization rate profile at $\omega t = 2\pi$ is presented in Fig. 8. The maximum is found in the beginning of the bulk plasma (i.e., at approximately 1 mm from the rf electrode) and decreases towards the cell walls. This profile is very similar to the ionization rate profiles obtained in the dc case. Furthermore, the other collision rates calculated at various times in the rf cycle show a similar profile, with a maximum in the beginning of the bulk plasma, and therefore, they are not shown here.

3.5 *Effect of previous rf cycles in the Monte Carlo model*

As discussed above, it was necessary to investigate how many rf cycles had to be followed with the Monte Carlo model before the periodic steady state was reached, and the effect of all electrons originating from previous rf cycles is thereby taken into account. Figure 9 shows the number of electrons and superelectrons simulated with our Monte Carlo model during three successive rf cycles. At $\omega t = 0$, the model starts with only a limited number of electrons at the rf electrode (3700 in this example). However, the number of electrons multiplies rapidly due to ionization collisions, which are very efficient around $\omega t = 0 = 2\pi$ (see Fig. 7). At $\omega t \sim \pi/4$, approximately 360,000 electrons (and superelectrons) are present in the plasma. Since the number of ionization collisions is, however, very low around $\omega t = \pi/2$, and since a lot of electrons disappear at this time from the Monte Carlo calculations because of their low energy, determined by ftoss (see above), the number of electrons decreases to ap-

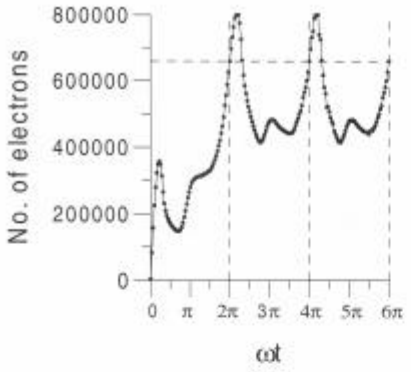

Fig. 9. Number of electrons (and superelectrons) followed in the Monte Carlo model as a function of time, during three successive rf cycles ($p = 6$ Torr, $P = 10$ W).

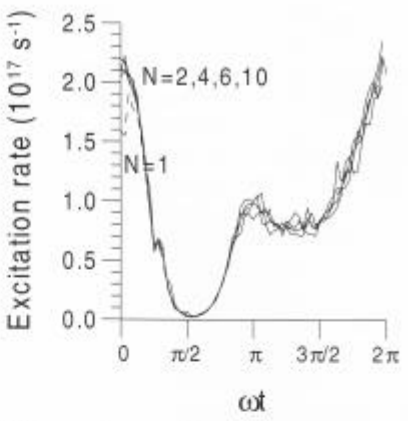

Fig. 10. Total electron impact excitation rate, integrated over the entire discharge volume, as a function of time in the rf cycle when following 1 (dashed line), 2, 4, 6 and 10 rf cycles (solid lines) ($p = 6$ Torr, $P = 10$ W).

proximately 150.000 around $\omega t = \pi/2$. However, as soon as the rf electrode again becomes negative and the ionization collisions are again more frequent, the number of electrons rises again around $\omega t = \pi$, and then stays more or less constant until $\omega t = 3\pi/2$, but then increases considerably to values on the order of 660,000 at $\omega t = 2\pi$.

When the second rf cycle starts, the number of electrons rises further since the ionization collisions are still very efficient, but then it drops again, due to the low number of ionization collisions and the rather high removal rate of electrons (and the transformation into superelectrons). Somewhat before $\omega t = 3\pi (= 2\pi + \pi)$ the ionization again becomes important, and the number of electrons increases at this point slightly, but it decreases again to a second minimum around $\omega t = 2\pi + 3\pi/2$, whereafter it starts to rise considerably once more as the ionization again becomes high. It can be observed in Fig. 9 that at the end of the second rf cycle, nearly the same number of electrons is present as at the end of the first rf cycle. Further time evolution of the number of electrons, in the third and in later rf cycles, is exactly the same as in the second rf cycle. This demonstrates that the periodic steady state is already reached in the second rf cycle, at the discharge conditions under investigation.

The same feature is illustrated in Fig. 10, which shows the total number of electron impact excitation collisions as a function of time in the rf cycle, when 1, 2, 4, 6 and 10 rf cycles are simulated. The result when following 1 rf cycle is denoted by the dashed line, whereas the other calculated values are depicted by the solid lines. It is seen that all solid lines coincide with each other, which demonstrates that following the electrons during 2, 4, 6 or 10 rf cycles yields the same results. The dashed line, on the other hand, deviates from the other curves until approximately $\omega t = \pi/4$, but further in the rf cycle, it coincides with the other lines. This also indicates that the periodic steady state is already attained at the second rf cycle.

4. Conclusions

A hybrid Monte Carlo-fluid model has been developed, to describe the behavior of the electrons and argon ions in a capacitively coupled rf glow discharge. Moreover, Poisson's equation is included in the fluid model to calculate the potential and electric field, which are required in the Monte Carlo model to define the trajectory of the electrons.

The input data for the model are the cell geometry, the gas pressure and discharge power, as well as the collision cross sections. The typical results determined include the rf and dc bias voltages, the spatial potential distribution, the position of the interface between the rf sheath and the bulk plasma, the electrical current, the densities of argon ions and electrons, the electron energy and the collision rates of the various collision processes. These results are presented here as a function of the two-dimensional position in the discharge and time in the rf cycle. In future research, we plan to perform some experiments, to check the modeling results.

Moreover, it was investigated as to how many rf cycles need to be followed in the Monte Carlo model before the periodic steady state is reached, and the previous rf cycles ceased to affect the present rf cycle. It was found that the periodic steady state was already reached at the second rf cycle.

Acknowledgments

A. Bogaerts is indebted to the Flemish Fund for Scientific Research (FWO-Flanders) for financial support. A. Bogaerts and R. Gijbels also acknowledge the financial support from the Federal Services for Scientific, Technical and Cultural Affairs (DWTC/SSTC) of the Prime Minister's Office through IUAP-IV (Conv. P4/10). The research of W. Goedheer is financed by the "Stichting voor Fundamenteel Onderzoek der Materie". Lastly, the authors wish to thank V. Hoffmann and I. Kaganovich for the interesting discussions.

1) *Glow Discharge Spectroscopies*, ed. R. K. Marcus (Plenum Press, New York, 1993).
2) *Glow Discharge Optical Emission Spectrometry*, eds. R. Payling, D. Jones and A. Bengtson (Wiley, Chichester, 1997).
3) S. De Gendt, R. Van Grieken, S. K. Ohorodnik and W. W. Harrison: Anal. Chem. **67** (1995) 1026.
4) M. J. Heintz and G. M. Hieftje: Spectrochim. Acta B **50** (1995) 1125.
5) M. R. Winchester and R. K. Marcus: Spectrochim. Acta B **51** (1996) 839.
6) V. Hoffmann, H.-J. Uhlemann, F. Präßler, K. Wetzig and D. Birus: Fresenius' J. Anal. Chem. **355** (1996) 826.
7) R. Jäger, J. S. Becker, H.-J. Dietze and J. A. C. Broekaert: Fresenius' J. Anal. Chem. **358** (1997) 214.
8) M. Fernandez, N. Bordel, R. Pereiro and A. Sanz-Medel: J. Anal. At.

Spectrom. **12** (1997) 1209.
9) M. Parker, M. L. Hartenstein and R. K. Marcus: Spectrochim. Acta B **52** (1997) 567.
10) D. A. Glocker and S. I. Shah: *Handbook of Thin Film Process Technology* (IOP Publishing, Bristol and Philadelphia, 1995).
11) M. A. Lieberman and M. A. Lichterberg: *Principles of Plasma Discharges and Materials Processing* (Wiley, New York, 1994).
12) A. Bogaerts, M. van Straaten and R. Gijbels: Spectrochim. Acta B **50** (1995) 179.
13) A. Bogaerts, M. van Straaten and R. Gijbels: J. Appl. Phys. **77** (1995) 1868.
14) A. Bogaerts, R. Gijbels and W. J. Goedheer: J. Appl. Phys. **78** (1995) 2233.
15) A. Bogaerts and R. Gijbels: Phys. Rev. A **52** (1995) 3743.
16) A. Bogaerts and R. Gijbels: J. Appl. Phys. **78** (1995) 6427.
17) A. Bogaerts and R. Gijbels: J. Appl. Phys. **79** (1996) 1279.
18) A. Bogaerts, R. Gijbels and W. J. Goedheer: Anal. Chem. **68** (1996) 2296.
19) A. Bogaerts and R. Gijbels: Anal. Chem. **68** (1996) 2676.
20) A. Bogaerts and R. Gijbels: Anal. Chem. **69** (1997) 719A.
21) A. Bogaerts, R. Gijbels and J. Vlcek: J. Appl. Phys. **84** (1998) 121.
22) A. Bogaerts, R. Gijbels and R. J. Carman: Spectrochim. Acta B **53** (1998) 1679.
23) V. A. Godyak and N. Sternberg: Phys. Rev. A **42** (1990) 2299.
24) S. V. Berezhnoi, I. D. Kaganovich, L. D. Tsendin and V. A. Schweigert: Appl. Phys. Lett. **69** (1996) 2341.
25) Y. T. Lee, M. A. Lieberman, A. J. Lichtenberg, F. Bose, H. Baltes, R. Patrick: J. Vac. Sci. & Technol. A **15** (1997) 113.
26) J.-P. Boeuf: Phys. Rev. A **36** (1987) 2782.
27) P. Belenguer and J. P. Boeuf: Phys. Rev. A **41** (1990) 4447.
28) M. Meyyappan and T. R. Govindan: IEEE Trans. Plasma Sci. **19** (1991) 122.
29) J. D. P. Passchier and W. J. Goedheer: J. Appl. Phys. **73** (1993) 1073.
30) F. F. Young and C. J. Wu: J. Appl. Phys. **74** (1993) 839.
31) M. Meyyappan and T. R. Govindan: J. Appl. Phys. **74** (1993) 2250.
32) J. D. P. Passchier and W. J. Goedheer: J. Appl. Phys. **74** (1993) 3744.
33) G.-J. Nienhuis, W. J. Goedheer, E. A. G. Hamers, W. G. J. H. M. van Sark and J. Bezemer: J. Appl. Phys. **82** (1997) 112.
34) M. A. Sobolewski: Phys. Rev. E **56** (1997) 1001.
35) T. J. Sommerer, W. N. G. Hitchon, R. E. P. Harvey and J. E. Lawler: Phys. Rev. A **43** (1991) 4452.
36) M. J. Kushner: J. Appl. Phys. **54** (1983) 4958.
37) M. J. Kushner: IEEE Trans. Plasma Sci. **14** (1986) 188.
38) P. W. May, D. Field and D. F. Klemperer: J. Appl. Phys. **71** (1992) 3721.
39) M. Surendra and D. B. Graves: IEEE Trans. Plasma Sci. **19** (1991) 144.
40) C. Li and C.-H. Wu: IEEE Trans. Plasma Sci. **20** (1992) 1000.
41) V. V. Ivanov, A. M. Popov, T. V. Rakhimova: Plasma Phys. Rep. **21** (1995) 692.
42) V. Vahedi and M. Surendra: Comput. Phys. Commun. **87** (1995) 179.
43) D. P. Lymberopoulos and D. J. Economou: J. Phys. D **28** (1995) 727.
44) T. H. Chung, H. J. Yoon, T. S. Kim, J. K. Lee: J. Phys. D **29** (1996) 1014.
45) H. B. Smith, C. Charles, R. W. Boswell and H. Kuwahara: J. Appl. Phys. **82** (1997) 561.
46) N. Sato and H. Tagashira: IEEE Trans. Plasma Sci. **19** (1991) 102.
47) T. J. Sommerer and M. J. Kushner: J. Appl. Phys. **71** (1992) 1654.
48) J.-H. Tsai and C.-H. Wu: J. Phys. D **26** (1993) 496.
49) K. Satake, T. Monaka, O. Ukai, Y. Takeuchi and M. Murata: Jpn. J. Appl. Phys. **36** (1997) 4789.
50) M. Surendra: Plasma Sources Sci. Technol. **4** (1995) 56.
51) F. Präßler, V. Hoffmann, J. Schumann and K. Wetzig: J. Anal. At. Spectrom. **10** (1995) 677.
52) V. Hoffmann: private communication.
53) G. Marsaglia and A. Zaman: Comput. Phys. **8** (1994) 117.
54) A. V. Phelps and Z. Lj. Petrovic: submitted to Plasma Sources Sci. & Technol.
55) S. Hashiguchi: IEEE Trans. Plasma Sci. **19** (1991) 297.
56) B. Chapman: *Glow Discharge Processes* (Wiley, New York, 1980).
57) J. P. Boeuf and E. Marode: J. Phys. D **15** (1982) 2169.
58) R. J. Carman: J. Phys. D **22** (1989) 55.
59) J. B. Hasted: *Physics of Atomic Collisions* (Butterworth, London, 1972).
60) M. Surendra, D. B. Graves and G. M. Jellum: Phys. Rev. A **41** (1990) 1112.
61) Y. Weng and M. J. Kushner: Phys. Rev. A **42** (1990) 6192.
62) N. R. Whetten, R. C. Weast and M. J. Astle: *CRC Handbook of Chemistry and Physics* (CRC, Boca Raton, 1982) 63rd ed., p. E-372.
63) L. Reimer: *Scanning Electron Microscopy* (Springer, Berlin, 1985).
64) A. Fiala: Dr. Thesis, Center for Plasma Physics and Their Applications, University Paul Sabatier of Toulouse, Toulouse, 1995.
65) D. Passchier: Dr. Thesis, Dept. Phys. University of Utrecht, Utrecht, 1994.
66) P. J. Chantry: J. Appl. Phys. **62** (1987) 1141.
67) H. K. Gummel: IEEE Trans. Electron. Devices **11** (1964) 455.
68) D. L. Scharfetter and H. K. Gummel: IEEE Trans. Electron. Devices **16** (1969) 64.
69) W. J. Goedheer, P. M. Meijer, J. Bezemer, J. D. P. Passchier and W. G. J. H. M. van Sark: IEEE Trans. Plasma Sci. **23** (1995) 644.
70) A. Bogaerts and R. Gijbels: Spectrochim. Acta B **53** (1998) 437.